Kinetic Study of Selective CO Oxidation over Pt-Co-Ce/Al$_2$O$_3$ Catalyst in Hydrogen-Rich Streams

Göktuğ Nezihi ÖZYÖNÜM[1], Ayşe Nilgün AKIN[2] and Ramazan YILDIRIM[1*]
[1]*Department of Chemical Engineering, Boğaziçi University, 34342 Bebek, İstanbul-TURKEY*
[2]*Department of Chemical Engineering, Kocaeli University, 41040 Kocaeli-TURKEY*
e-mail: yildirra@boun.edu.tr

The kinetics of the selective CO oxidation was studied in a fixed-bed microreactor at atmospheric pressure over Pt-Co-Ce/Al$_2$O$_3$ catalyst, which was prepared using the incipient to wetness co-impregnation technique. Intrinsic kinetic data were obtained in the initial rate region using 8 different sets of CO and O$_2$ concentrations, each at 2 space times, i.e. 2 catalyst loadings, at 110 °C. The kinetic models based on elementary reaction steps were constructed and tested using nonlinear regression analysis with Levenberg-Marquardt algorithm. The alternative models proposed for the similar catalytic systems in the literature were also tested. It was found that Pt-Co-Ce/Al$_2$O$_3$ acts as a bifunctional catalyst (assuming ceria and cobalt sites are identical) and the reactions proceed via a Langmuir-Hinshelwood (L-H) type mechanism. However, no further discrimination could be made among the models based on bifunctionality and L-H kinetics. An empirical power law model was also tested and the results were found to be quite satisfactory.

Key Words: CO oxidation, Pt-Co-Ce/Al$_2$O$_3$ catalyst, kinetic study, reaction mechanism.

Introduction

Proton-exchange membrane (PEM) fuel cell is an attractive energy conversion device, particularly for small-to medium-scale stationary and mobile applications. However, the hydrogen stream from the fuel processor usually contains 0.5%-1% CO, which poisons the anode catalyst of the fuel cell even at trace levels.[1] The preferential CO oxidation (PROX) is considered one of the most feasible methods to clean hydrogen streams from CO.[2]

Supported platinum-based catalysts have been considered particularly for the elimination of carbon monoxide in hydrogen-rich streams.[3−5,9−12] A range of noble metal reducible oxide (NMRO) catalysts including Pt-Sn, Pt-Fe, Pt-Co, and Pt-Ce combinations have been proposed as promising choices for CO removal from either hydrogen-rich or oxygen-rich gas streams.[3]

---

[*]Corresponding author

The CO oxidation over Pt-Co-Ce/γ-Al$_2$O$_3$ catalyst in hydrogen-rich streams was studied in our laboratory using a realistic gas composition of 60% H$_2$, 25% CO$_2$, 10% H$_2$O, 1% O$_2$, 1% CO, and He as balance. The effects of catalyst preparation and reaction conditions were investigated and reported in a previous communication.[4] It was found that 1.4 wt% Pt-1.25 wt% Co-1.25 wt% Ce /γ-Al$_2$O$_3$ catalyst is very effective to remove CO from the hydrogen stream at 110 °C.[4] Hence, the kinetics of CO oxidation over this catalyst was studied in the present work to further understand and improve the performance of Pt-Co-Ce/γ-Al$_2$O$_3$ catalysts.

Experimental

Pt-Co-Ce/Al$_2$O$_3$ catalysts containing 1.4 wt.-% Pt and 1.25 wt.-% Co and Ce were prepared using the classical incipient to wetness co-impregnation technique. The detailed preparation procedure is given elsewhere.[4]

Kinetic measurements were obtained using a microreactor flow system. Research grade CO, O$_2$, H$_2$, CO$_2$, and He were used and their flow rates were controlled using Brooks 5850E and/or Aalborg DFC2600 mass flow controllers. The water was pumped into the preheated (150 °C) reactant gas mixture using a Jasco PU-2080Plus HPLC pump and it was evaporated in a glass wool bed before reaching the catalyst. The feed mixture was allowed to flow through the 4 mm i.d. stainless steel fixed-bed reactor. Reactor temperature was controlled by a Shimaden FP-21 programmable controller in a 40 cm × 2.4 cm i.d. tube furnace. Product streams were analyzed using a Shimadzu GC-8A gas chromatograph connected to a Shimadzu CR-4A data processor and Molecular Sieve 5A (60-80 mesh). CO and O$_2$ concentrations were determined by chromatographic analysis while the CO$_2$ concentration was calculated using carbon balance, assuming that all the carbon reacted was converted to CO$_2$ and considering that no additional peak was observed in chromatograms.

In order to keep the conversions at low values, small amounts of catalyst, e.g., 10 mg or 20 mg, were put into the reactor. To minimize axial dispersion, the catalyst bed was diluted using inert γ-Al$_2$O$_3$ such that the total bed weight remained constant at 250 mg. The total flow rate was kept at 100 mL/min for all reactions and 45-60 mesh size (344-255 μm particle size) was used. The catalyst samples used in the experiments were reduced in situ at 375 °C in a hydrogen environment for 3 h before each kinetic measurement. The CO conversion was measured at the time on stream of 60 min (after the reactant gases were introduced to the system), which should be sufficient to reach the steady state conditions.

Results and Discussion

Reaction Mechanisms

Several mechanisms based on elementary reactions were constructed and those mechanisms were listed as alternative reaction paths in Table 1. No distinction was made between the cobalt and the ceria sites for simplicity, and both are labeled as "s" in Table 1. CO$_2$, H$_2$O, and H$_2$ were also not considered explicitly in modeling as their effects on the reaction rates were assumed to be by means of a change in the rate parameters but not in the reaction mechanism. This should be a reasonable assumption since it is reported that the effects of approximately 10% CO$_2$ and H$_2$O in the feed on CO oxidation are quite small.[5] Rajasree et al.[6] stated that CO$_2$ inhibits the CO oxidation by decreasing the oxygen storage capacity (OSC), and

decreases the concentration of adsorbed oxygen on OSC hindering the interface reaction between the noble metal and the OSC. The elementary steps involving this effect, however, were already covered in Table 1. Finally Kim and Lim[7] reported that H_2 does not affect the CO conversion as long as the feed contains more than 10% H_2, which is the case in this study.

Table 1. Elementary reaction paths considered in the kinetic modeling of CO oxidation over Pt-Co-Ce/Al$_2$O$_3$.

Elementary Step	Reaction Path					Step Number
	A	B	C	D	E	
	$^a\sigma_A$	σ_B	σ_C	σ_D	σ_E	
$CO + * \underset{k_1^b}{\overset{k_1^f}{\Leftrightarrow}} CO*$	2	0	2	1	4	(1)
$CO + s \underset{k_2^b}{\overset{k_2^f}{\Leftrightarrow}} COs$	0	0	0	1	0	(2)
$O_2 + * \overset{k_3^f}{\rightarrow} O_2*$	1	1	0	0	1	(3)
$O_2* + * \overset{k_4^f}{\rightarrow} 2O*$	1	1	0	0	1	(4)
$O_2 + s \overset{k_5^f}{\rightarrow} O_2s$	0	0	1	1	1	(5)
$O_2s + s \overset{k_6^f}{\rightarrow} 2Os$	0	0	1	1	1	(6)
$CO + O* \underset{k_7^b}{\overset{k_7^f}{\Leftrightarrow}} OCO*$	0	2	0	0	0	(7)
$OCO* \overset{k_8^f}{\rightarrow} CO_2 + *$	0	2	0	0	0	(8)
$CO* + O* \overset{k_9^f}{\rightarrow} CO_2 + 2*$	2	0	0	0	2	(9)
$CO* + Os \overset{k_{10}^f}{\rightarrow} CO_2 + * + s$	0	0	2	1	2	(10)
$COs + Os \overset{k_{11}^f}{\rightarrow} CO_2 + 2s$	0	0	0	1	0	(11)
$2nCO + nO_2 \rightarrow 2nCO_2$	(Net Reaction)					

$^a\sigma_i$: stoichiometric coefficients for elementary steps in path i

Modeling

The surface concentrations of the surface species were evaluated from the corresponding continuity equations by employing the steady state assumption.

$$\sum_{j=1}^{N} v_{i,j} r_{w,j} = 0 \tag{1}$$

where j corresponds to the number of reaction steps, while N is the total number of reaction steps, $v_{i,j}$ represents the stoichiometric coefficient of species i in the reaction j, and $r_{w,j}$ is the reaction rate of step j in $\mu mol\ mg_{CAT}^{-1}\ s^{-1}$. The reaction rates for the elementary steps were calculated from the mass balance with the assumptions of the identical active sites, the absence of the interactions between adsorbates, and the monolayer surface coverage.[5]

In the monofunctional reaction path A, in which all the active sites were assumed to be the same, oxygen adsorption is thought to proceed in 2 steps in series: first the irreversible molecular chemisorption of O_2, followed by the dissociation of O_2* on the noble metal, i.e. steps (3) and (4) in Table 1. Although

O_2 adsorption was found to proceed dissociatively at temperatures above 100 K, molecularly adsorbed O_2 is often included in the reaction mechanisms.[5,8] CO_2 formation takes place via a Langmuir-Hinshelwood surface reaction, i.e. step (9). In the case of adsorption equilibrium for CO, the rate expression for the reaction path A is simplified to Eq. (2).

$$-r_{CO} = \frac{(2k_3^f P_{O_2})(K_1 k_4^f k_9^f P_{CO} [S]_0 - K_1 k_3^f k_9^f P_{CO} P_{O_2} - 2k_3^f k_4^f P_{O_2})}{K_1 k_4^f k_9^f P_{CO}(K_1 P_{CO} + 1)} \tag{2}$$

where $k's$ and $K's$ are rate and equilibrium constants of reaction steps, respectively, while $P's$ represent the partial pressure of gas phase species and $[S]_o$ is the initial active site concentration for Pt.

Reaction path B is also a monofunctional path that takes place via the Eley-Rideal step between adsorbed oxygen and gas phase CO comprising the formation of the OCO* surface species on platinum, step (7) in Table 1. The OCO* species can either desorb, leading to O* on the noble metal surface and CO in the gas phase, or react to CO_2.[9] Assuming that the molecular chemisorption of oxygen is rate determining, i.e. $k_4^f >> k_3^f$, the rate expression for the reaction path B takes the following form:

$$-r_{CO} = \frac{2k_3^f k_7^f k_8^f P_{CO} P_{O_2} [S]_0}{2k_3^f P_{O_2}(k_7^f + k_8^f) + k_7^f k_8^f P_{CO} + 2k_3^f k_7^f P_{CO} P_{O_2}} \tag{3}$$

Reaction path C is a bifunctional reaction path, involving O_2 adsorption on the cobalt-ceria surface, i.e. steps (5) and (6) in Table 1, and a reaction between CO adsorbed on the noble metal surface and oxygen from cobalt-ceria at the noble metal/cobalt-ceria interface, i.e. step (10). The cobalt-ceria sites involved in the reaction path C are referred to as OSC sites and are denoted by "s", which can be the sites on top of the cobalt-ceria lattice, or more likely the oxygen vacancies at the surface of the cobalt-ceria lattice. Oxygen atoms become available for reaction at the noble metal/cobalt-ceria interface directly by adsorption from the gas phase via surface diffusion of the oxygen adsorbed on the cobalt-ceria surface. Bulk diffusion becomes kinetically significant only at high temperatures.[9] Assuming that the noble metal surface is completely covered with CO, and O_2 chemisorption is potentially slow, as compared to its dissociation, implying $k_6^f >> k_5^f$, the rate expression for the reaction path C is simplified to Eq. (4).

$$-r_{CO} = \frac{2k_5^f k_{10}^f P_{O_2} [S]_0 [V]_0}{2k_5^f P_{O_2} + k_{10}^f [S]_0} \tag{4}$$

where $[V]_o$ is the initial concentration of Co-Ce active sites.

Reaction path D is a bifunctional path in which the gas-phase CO is adsorbed reversibly on both the noble metal and cobalt-ceria sites, i.e. steps (1) and (2). It is known that a considerable amount of CO is adsorbed on the cobalt sites over cobalt-containing catalysts.[10,11] O_2 adsorption is thought to proceed in 2 consecutive steps on cobalt-ceria sites and CO_2 formation takes place via 2 Langmuir-Hinshelwood surface reactions: one with the adsorbed CO on the noble metal[12,13], and the other with the adsorbed CO on the cobalt-ceria sites.[14] Assuming that CO* is the most abundant reaction intermediate, i.e. [COS]>>[S], and CO adsorption on the cobalt-ceria sites is in equilibrium, and additionally that O_2 chemisorption is potentially slower than its dissociation, implying $k_6^f >> k_5^f$, the rate expression for the reaction path D comes into its final form as below:

$$-r_{CO} = \frac{2k_5^f P_{O_2} [V]_0}{K_2 P_{CO} + 1} \tag{5}$$

In the bifunctional reaction path E, the noble metal adsorbs both CO and oxygen. Oxygen is adsorbed also by the cobalt-ceria sites, i.e. steps (5) and (6) in Table 1. CO_2 formation is thought to proceed via 2 individual Langmuir-Hinshelwood surface reactions: one with the dissociated oxygen on the noble metal, i.e. step (9), and the other with the dissociated oxygen on the cobalt-ceria sites, i.e. step (10). With the assumption of CO adsorption equilibrium on the noble metal, and that the molecular adsorption of oxygen on the noble metal is rate determining implying that k_3^f is too small, and O_2 chemisorption on cobalt-ceria sites is potentially slower as compared to its dissociation, i.e. $k_6^f >> k_5^f$, the rate expression for the reaction path E simplifies to Eq. (6).

$$-r_{CO} = \frac{2k_3^f P_{O_2} [S]_0}{K_1 P_{CO} + 1} + \frac{K_1 k_{10}^f P_{CO} [S]_0 [V]_0}{K_1 P_{CO} [S]_0 + K_1 P_{CO} + 1} \tag{6}$$

Regression Analysis

The Levenberg-Marquardt regression scheme provided in the LSQNONLIN subroutine function in computer software MATLAB v.7.0.4[15] was used for nonlinear regression analysis.

Rate Calculations

Rates of CO consumption were evaluated using the differential method. The experimental conditions were fixed to keep the CO conversions at low values, e.g., less than 20% for the differential reactor approximation[16,17], and it was tried to make the conversion even less than 10% if possible.[5,7]

The kinetic experiments were repeated for 8 different feed compositions at 110 °C, each at 2 different space times, to ensure that the data correspond to the linear change of CO conversion (X_{CO}) with space time (W/F_{CO}) in the initial rates region in which the reaction is kinetically controlled. The rate data are given in Table 2.

Table 2. Reaction rates calculated from W_{CAT}/F_{CO} versus X_{CO} at T = 110 °C.

Exp. no.	CO (mol %)	O_2 (mol %)	[a]W_{CAT} / [b]F_{CO} (mg.s.μmol^{-1})	[c]X_{CO} (fractional)	Reaction rate ($\mu mol\ mg^{-1}s^{-1}$)
1	1	0.5	18.868	0.032	0.0023
2			37.736	0.094	
3	1	0.75	18.868	0.063	0.0028
4			37.736	0.102	
5	1	1	18.868	0.079	0.0034
6			37.736	0.121	
7	1	1.25	18.868	0.081	0.0039
8			37.736	0.142	
9	1	1.5	18.868	0.088	0.0041
10			37.736	0.149	
11	0.75	1	25.157	0.087	0.0040
12			50.314	0.211	
13	1.25	1	15.094	0.058	0.0033
14			30.189	0.096	
15	1.5	1	12.579	0.048	0.0031
16			25.157	0.075	

[a]Catalyst weight, [b]CO flow, [c]CO conversion

Model Discrimination

The criterion often used in model discrimination requires that the parameters of the rate equation be positive. Statistical fitness of the calculated rate values with the experimental data is also tested for model discrimination.

The determination of all the constants in the model equations would not be feasible since it would require a large number of experiments. Hence the constants in each model equation were combined as much as possible to minimize the number of unknowns and, therefore, the number of experimental data required. After the regression analysis, only the reaction pathways C (Eq. (4)) and D (Eq. (5)) passed the requirement of having positive rate and equilibrium parameters. The final forms of the Eqs. (4) and (5) with the combined constants (as well as with the calculated values of these constants by regression) are given below as Eqs. (4*) and (5*), respectively:

$$-r_{CO} = \frac{K_1 P_{O_2}}{K_2 P_{O_2} + 1} = \frac{6.66 \times 10^{-6} P_{O_2}}{9.65 \times 10^{-4} P_{O_2} + 1} \qquad 4*$$

$$-r_{CO} = \frac{K_1 P_{O_2}}{K_2 P_{CO} + 1} = \frac{3.5 \times 10^{-6f} P_{O_2}}{8.31 \times 10^{-4} P_{CO} + 1} \qquad 5*$$

Then the experimental versus calculated rates were plotted to further analyze and discriminate the fitness of these 2 models in Figure 1. The plot in Figure 1 was constructed by setting the intercept to zero in accordance with the physical reality although the R^2 value is significantly higher if the value of intercept is not set.
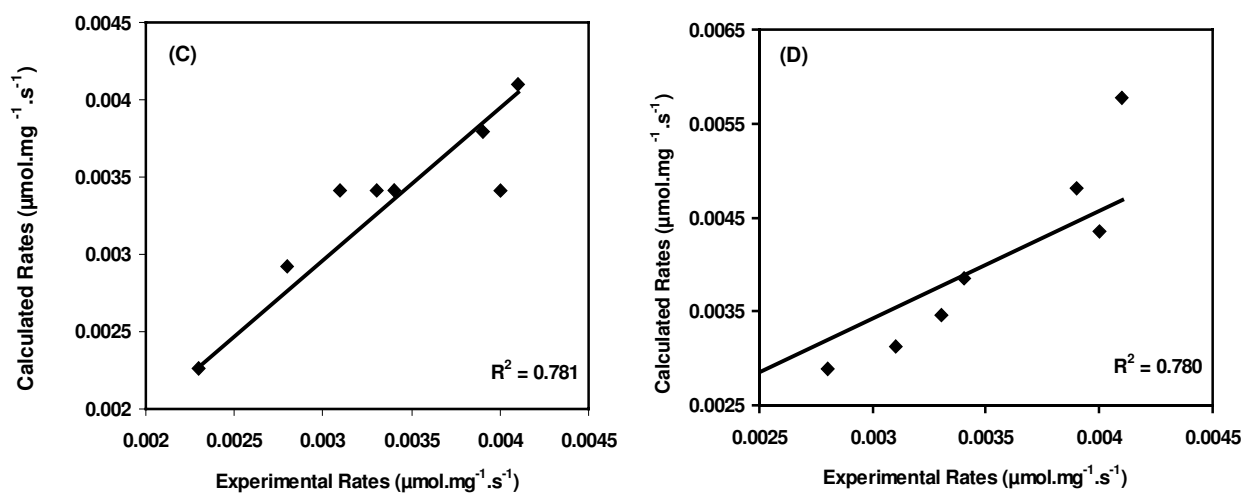

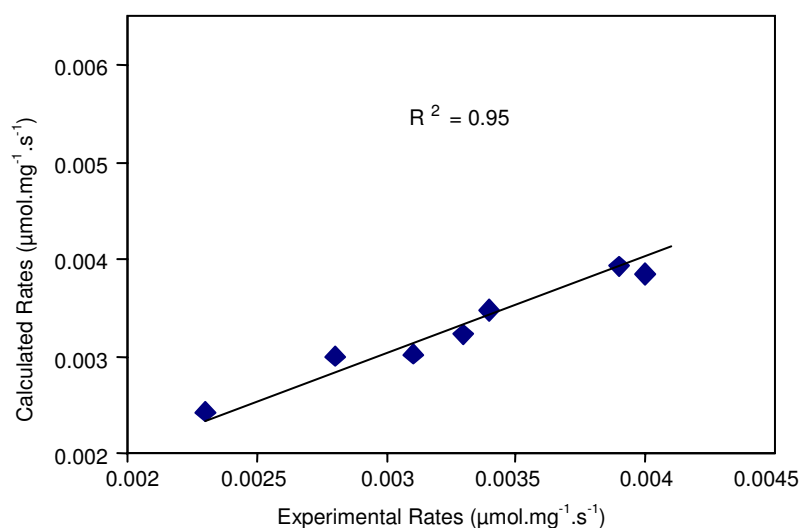**Figure 1.** Experimental versus calculated rates for model C (Eq. (4)) and D (Eq. (5)).

Both models represent the experimental data reasonably well, although none of them is successful enough to draw any conclusions about the exact nature of the mechanisms. However, both models suggest the presence of bifunctional mechanisms and Langmuir-Hinshelwood type kinetics. This result was also verified when the data were compared to the models suggested for similar reaction mechanisms in the literature.[5,18] On the other hand, there is a significant difference between 2 models in terms of CO dependency. Although the rate depends only on the oxygen concentration in model C (Eqs. (4) and (4*)), model D (Eqs. (5) and

(5*)) indicates some CO dependency. No further discrimination could be made between the models since R^2 values for calculated versus experimental rate plot are the same (0.78) for both models, indicating the same level of statistical fit. However, a model equation containing only a partial pressure of CO, which was proposed for $Pt-CeO_2/Al_2O_5$ by Oran and Üner, did not fit the experimental data well.[19]

Due to the limitation of elementary models discussed above, a power law model was also constructed to have some empirical expression for the rate equation. The following model equation was found to represent the experimental data very well within the experimental conditions as indicated by the plot of experimental versus calculated rates in Figure 2.

$$-r_{CO} = 0.001 \, (P_{CO})^{-0.35} \, (P_{O_2})^{0.53} \tag{7}$$

The negative dependency of the rate on CO concentration and the positive effects of O_2 concentration are in agreement with similar studies in the literature.[20,21] Although the power law model seems to support model D against model C in terms of negative CO dependency, the results are still not conclusive.

Figure 2. Experimental versus calculated rates for the power law model (Eq. (8)).

Since the power law model represented the experimental results well, Arrhenius parameters were also determined by repeating some experiments at 2 other reaction temperatures. The experimental conditions and rate data for those experiments are given in Table 3.

Table 3. Reaction rates and corresponding reaction constant as a function of temperature for the power law model in Eq. (7). The feed composition: 1% CO, 0.5% O_2, 25% CO_2, 10% H_2O measured at 60% H_2, and balance He.

Temperature (°C)	[a]W_{CAT} / [b]F_{CO} (mg.s.μmol^{-1})	[c]X_{CO} (fractional)	Reaction rate (μmol.mg^{-1}s^{-1})	k (μmol.mg^{-1}s^{-1}Pa$^{-0.18}$)
110	18.868	0.032	0.0023	0.0010
110	37.736	0.094		
120	18.868	0.066	0.0039	0,0016
120	37.736	0.149		
130	18.868	0.093	0.0047	0,0020
130	37.736	0.176		

[a]Catalyst weight, [b]CO flow, [c]CO conversion

The Arrhenius plot between ln$k$ versus 1/T resulted in a significantly good fit as indicated by the relatively high R^2 value of 0.967 (Figure 3). The apparent activation energy was found to be 24.79 kJ/mol while the pre-exponential factor A was calculated as 39.17 μmol.mg^{-1}.s^{-1}.Pa$^{-0.18}$ at the temperature range of 110-130 °C. It should be noted that the activation energy calculated from Figure 3 is just an apparent activation energy and it is purely empirical. Hence its relatively small value (as it suggests physical adsorption) should not have any physical meaning.
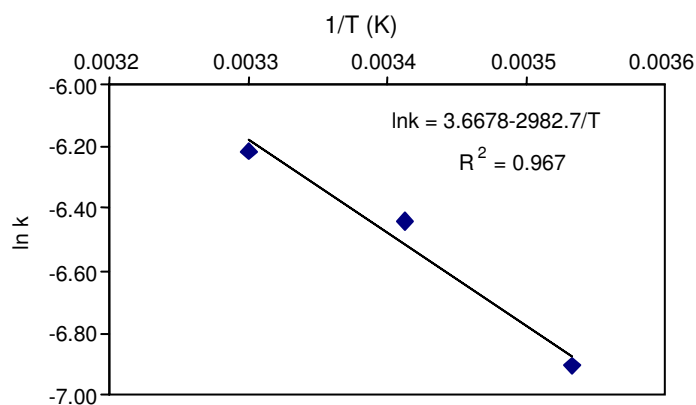

Figure 3. Arrhenius plot for the power law model.

Conclusions

It can be concluded that the CO oxidation over Pt-Co-Ce/Al$_2$O$_3$ proceeds with Langmuir-Hinshelwood type mechanisms in which Pt-Co-Ce/Al$_2$O$_3$ acts as a bifunctional catalysis. No further discrimination could be made using the data obtained in this work. It should be noted that the "bifunctional" catalyst assumption is also a simplification. Co sites are not exactly identical to Ce sites since Co also adsorbs CO.[11] Similarly, it is also known that Pt is active for O$_2$ adsorption as can be seen in various studies of CO oxidation over Pt catalyst in the absence of any metal oxide promoter.[3] The power law function, on the other hand, represents the experimental data reasonably well within the conditions studied and it can be used for preliminary design studies although it is empirical.

Acknowledgments

References

1. Manasilp and E. Gulari, **Appl. Catal. B 37,** 17-25 (2002).

2. Y. Choi and H.G. Stenger, **J. Power Sources 129**, 246-254 (2004).

3. D.L. Trimm and Z.İ. Önsan, **Catal. Rev. 43 (1-2),** 31-84 (2001).

4. T. İnce, G. Uysal, A.N. Akın and R. Yıldırım, **Appl. Catal. A 292**, 171-176 (2005).

5. R.H. Nibbelke, M.A.J. Campman, J.H.B.J. Hoebink and G.B. Marin, **J. Catal. 171,** 358-373 (1997).

6. R. Rajasree, J.H.B.J. Hoebink and J.C. Schouten, **J. Catal. 223**, 36-43 (2004).

7. D.H. Kim and M.S. Lim, **Appl. Catal. A 224,** 27-38 (2002).

8. I. Manuel, J. Chaubet, C. Thomas, H. Colas, N. Matthess and G.D. Mariadassou, **J. Catal. 224**, 269-277 (2004).

9. R.H. Nibbelke, A.J.L. Nievergeld, J.H.B.J. Hoebink and G.B. Marin, **Appl. Catal. B 19**, 245-259 (1998).

10. A. Törncrona, M. Skoglundh, P. Thormählen, E. Fridell and E. Jobson, **Appl. Catal. B 14**, 131-145 (1997).

11. P. Thormählen, M. Skoglundh, E. Fridell and B. Andersson, **J. Catal. 188**, 300-310 (1999).

12. Y.J. Mergler, J.H.B.J. Hoebink and B.E. Nieuwenhuys, **J. Catal. 167**, 305-313 (1997).

13. T. Bunluesin, R.J. Gorte and G.W. Graham, **Appl. Catal. B 15**, 107-l 14 (1998).

14. J. Jansson, M. Skoglundh, E. Fridell and P. Thormählen, **Top. Catal. 16/17 No. 1-4**, 385-389 (2001).

15. MATLAB, Version 7.0.4, **The MathWorks Inc.,** USA, 2005.

16. N.W. Cant and N.J. Ossipoff, **Catal. Today 36**, 125-133 (1997).

17. Y.F. Han, M. Kinne and R.J. Behm, **Appl. Catal. B 52,** 123-134 (2004).

18. A.N. Akın, G. Kılaz, A.İ. İşli and Z.İ. Önsan, **Chem. Eng. Sci. 56**, 881-888 (2001).

19. U. Oran. D.Üner, **Appl. Catal B** 54, 183-191(2004).

20. M.J. Kahlich, H.A. Gasteiger and R.J. Behm, **J. Catal. 171,** 93-105 (1997).

21. B. Gülyüz, **"Kinetics of Low Temperature CO Oxidation over Activated Carbon Supported Pt-CeO$_x$ Catalyst"** MS Thesis, Boğaziçi University, Istanbul, Turkey, 2007.